An analytic model to study the radiative and thermodynamical properties of a corona around a compact object. II Feedback model

Jesse Roomer
Astronomy

July 8, 2022

kapteyn astronomical institute

An analytic model to study the radiative and thermodynamical properties of a corona around a compact object. II Feedback model

Author:	Jesse Roomer
Time period:	April 2022 - July 2022
Organization:	Kapteyn Astronomical Institute, University of Groningen
Department:	Faculty of Science and Engineering
Place and country:	Groningen, The Netherlands
Supervisor at Kapteyn:	Prof. Dr. R.M. Mendez
Date:	July 8, 2022

Abstract

A model is created for the escaping photon distribution of a corona around a compact object as a function of time and energy which includes feedback from the corona to the source. This model uses the exact closed-form expression for the time-dependent Green's function solution to the Kompaneets' equation found by Becker (2004)[2]. In a previously created model described in Roomer (2021)[24] it is assumed that no photons from the corona are going back into the black body. This model describes the evolution in energy space of a photon distribution with a varying injection rate or varying black body temperature. In a case where the photons would fall back into the source, the returning photons will change the temperature of the source, since they add energy to the black body. For a new, improved model, this feedback will be added to the model containing temperature oscillations from Roomer (2021)[24]. The model can be used to create light curves, spectra, power density spectra (PDS), phase lags, and root mean square (rms). Here, the PDS will show peaks, also known as quasi-periodic oscillations or QPOs which are also found in PDS of observations and can be used to compare to the data. Phase lags of the photons in the escaping photon distribution are caused by delays of the photons due to scattering in the corona. These phase lags can be reproduced by the model to compare with observations.
The feedback model is obtained for different oscillation frequency values. These different results are then compared. The width of one QPO in a PDS for one frequency has also been determined using a Lorentzian fit.

Used abbreviations

- FFT: Fast Fourier Transform
- FWHM: Full Width Half Maximum
- HMXB: High Mass X-ray Binary
- kHz QPO: Kilohertz quasi-periodic oscillations
- LF QPO: Low-frequency quasi-periodic oscillations
- LMXB: Low Mass X-ray Binary
- LTP: Lense-Thirring precession frequency
- PDS: Power density spectra
- QPO: Quasi-periodic oscillation
- rms: Root mean square
- RPM: Relativistic precession model
- SPBF: Sonic-point beat-frequency

Used symbols

- A: Amplitude [-]
- B_E: Specific intensity of black body $[erg \cdot cm^{-2} \cdot s^{-1} \cdot sr^{-1}]$
- B_x: Specific intensity of black body [-]
- $B_{x,0}$: Specific intensity of black body for the initial temperature [-]
- $B_{x,-1}$: Specific intensity of black body at time $t-1$ [-]
- c: Speed of light $[cm \cdot s^{-1}]$
- E: Energy $[keV]$
- ν: Frequency [Hz]
- ν_{esc}: Escape frequency $[s^{-1}]$
- h: Planck constant $[erg \cdot s]$
- k: Boltzmann constant $[erg \cdot K^{-1}]$
- kT_{bb}: Black body temperature $[keV]$
- kT_e: Electron temperature $[keV]$
- kT: Black body temperature in units of the electron temperature [-]
- L: Luminosity of black body $[erg \cdot s^{-1}]$
- m_e: Electron mass $[g]$
- n_e: Electron number density $[cm^{-3}]$

- $\dot{N}_x$: Number of photons escaping cloud per unit time, per energy [photons/second]
- $\dot{N}_0$: Injection rate of photons per unit time with dimensionless energy x_0 [photons/second]
- R: Radius of black body $[cm]$
- t_0: Initial time $[s]$
- t: Time $[s]$
- t_{esc}: Mean escape time of a photon $[s]$
- x: Energy [-]
- x_0: Initial energy [-]
- y: Compton y-parameter/dimensionless time [-]
- $\tilde{y}$: Mean value of Compton-y parameter [-]
- σ_T: Thomson cross-section $[cm^2]$
- σ: Stefan-Boltzmann constant $[erg \cdot K^{-4} \cdot cm^{-2} \cdot s^{-1}]$
- τ: Optical depth [-]
- ω: Angular frequency $[rad \cdot s^{-1}]$

Contents

1. Introduction

In a binary system containing a star and neutron star, the mass accreted from the star forms a disk around the neutron star. A corona containing electrons will also form around the neutron star. In this corona, photons from the neutron star and disk will scatter with the electrons in the corona. Figure 1 shows a schematic example. Note that the shape of the corona is currently a topic of research and the shape in Figure 1 is for the specific case of microquasar GRS 1915+105.

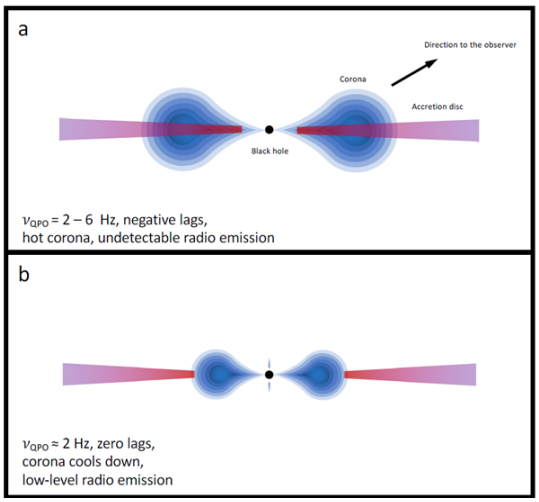

Figure 1: Corona around a compact object and its disc. Panel a shows a hot corona that covers part of the disc. In panel b the corona has cooled down and the size of the corona is equal to the inner radius of the disc. Taken from Mendez et al. (2022)[17].

A model to describe the number of photons leaving the corona as a function of time has been created in a previous research project.[24] In the previous project, a model described in a paper by Becker (2002)[2] has been recreated and extended to create an improved model. The paper obtains an exact closed-form expression for the time-dependent Green's function solution to the Kompaneets' equation. The Kompaneets' equation describes the spectral modification of a photon distribution as it moves through a hot electron population.[25] Green's function can be used to solve differential equations such as the Kompaneets' equation.[8] The solution obtained describes the evolution in energy space of a photon distribution that is initially monoenergetic.[2] The model of Becker (2002)[2] assumes that the corona and photon source (i.e. black body) will not change in temperature and that the source provides a constant injection of photons into the corona. In the previous project, either source temperature oscillations or injection rate oscillations were added to the model after recreating the results of the paper[2] in a Python model.[24]
However, a more accurate model contains both oscillations. In the previous model, it is assumed that no photons from the corona are going back into the black body. In a case where this would happen, the returning photons will change the temperature of the source since they add energy to the black body. Adding this feedback to the model will create an improved model. The goal of this project is to extend the previous model further to create an improved model to simulate the escaping photon distribution of a corona around a compact object. This will be done by adding feedback from the corona back to the black body on top of the temperature oscillations. With this model, the power density spectrum (PDS) can be created to simulate the quasi-periodic oscillations (QPOs), phase lags, and rms. Here, a PDS can be found by calculating the Fast Fourier Transform (FFT) of the light curves obtained. They can be useful to analyze the variability of a light curve of a source. A PDS will give the square

of the amplitude, also called power, of the variability of the light curve at each frequency.[16] Here, the light curves show the escaping photon distribution versus time. The phase lags will be explained further in section 2.1. As the name implies, the rms is the square root of the mean square. It will show the variability of the light curve of a source over a range of frequencies.[17] Using the PDS, the dependence of the width of the QPOs with frequency can be analyzed. The PDS, phase lags, and rms from the model can also be compared with results obtained from observations to give a better understanding of the QPOs and phase lags and their origin.

This report will start with a theoretical background on the subject in section 2. Section 3 will then describe the method and results for the new model and in section 4 the model will be discussed. Finally, in section 5 a conclusion of the research is provided, and in section 6 recommendations for the next steps.

2. Theoretical background

This section will provide background information on binary systems, the corona, the Kompaneets' equation, black body radiation, and quasi-periodic oscillations (QPOs). If one would prefer to have more information, it is advised to read the report by Roomer (2021)[24]. Some terms mentioned in this section are not further elaborated when they have no significant relevance to the research in this paper.

2.1. Binary systems

A binary system contains two objects orbiting around each other, where one of the two is a compact object and the other a star. The compact object can be either a neutron star, black hole, or white dwarf. Due to the gravity of the compact object, it can strip matter from its companion. The matter transfer can happen due to Roche lobe overflow or stellar wind accretion.[20] More information on the type of binary systems can be found in Roomer (2021)[24]. X-ray binaries are a special type of binary system. They emit X-ray radiation and can be divided into two classes: Low Mass X-ray Binaries (LMXB) and High Mass X-ray Binaries (HMXB). In LMXB the companion star has a lower mass than the mass of the compact object, while for HMXB the companion star has a mass that is higher than that of the compact object. The model created in this paper is a model for LMXB.
Mass transfer to the compact object will create a disk around it. Due to the loss in gravitational energy when falling towards the compact object, the disk will heat up. Heating of this disk causes a corona to form. Figure 1 shows a schematic picture of the corona.[7]

The corona contains electrons and can Compton-scatter, also called Comptonise, photons coming from the compact object and/or disk.[6] These photons can have high or low energies, depending on the number of times they have scattered. Photons with high energies are called hard photons and photons with low energies are soft photons. These soft photons thus have longer wavelengths and are produced when hard radiation from the corona falls in the accretion disc and is reflected or thermalized. The photons then enter the corona again and Compton cools the plasma.[24] The hard photons have a delay (also called time and phase lag) with respect to the soft photons since they undergo more scattering. The time lags are the time delays between these photons. They also have a phase lag due to this scattering. This is the phase of the averaged cross-power spectrum.[22]

2.2. Green function solution to the Kompaneets' equation

X-ray spectra show power-law tails due to thermal Comptonization. They also show time and phase lags between the observed photons because of this phenomenon. The Kompaneets' equation described in Rybicki(2004)[25] expresses this thermal Comptonization:

$$\frac{1}{n_e \sigma_T c}\frac{\partial n}{\partial t} = \left(\frac{kT}{mc^2}\right)\frac{1}{x^2}\frac{\partial}{\partial x}\left[x^2\left(n' + n + n^2\right)\right]. \tag{1}$$

It describes the spectral modification of a photon distribution as it moves through a hot electron population. The equation assumes that photons scatter off non-relativistic electrons and therefore the fractional energy transfer for each scattering is small.[25]
In the Kompaneets' equation, n' is the diffusion along the x-axis, n is the cooling of the photon population as the photons scatter on electrons that take part in the energy recoil, and n^2 is the stimulated reactions. n_e is the electron number density, σ_T the Thomson cross-section, c the speeds of light, k the Boltzmann constant, T the electron temperature, t the time and x the energy, given by

$$x = \frac{E}{kT_e}. \tag{2}$$

y is the Compton y-parameter given by

$$y = \frac{kT_e}{m_e c^2}\tau_T, \tag{3}$$

where τ_T is the optical depth.[25] When $y \ll 1$ the spectrum is a modified black body and when $y \gg 1$ the photons are in equilibrium or saturated Comptonization. In all other cases, the Kompaneets' equation is required.[2, 7]
Equation 1 can be solved using Green's function. A Green's function is the inverse of an arbitrary linear differential operator L.[8] It can be used to solve complicated differential equations and is fully explained in Roomer (2021)[24]. The Green's function solution to the Kompaneets' equation determined by Becker (2002)[2] is given by

$$f_G(x, x_0, y) = \frac{32}{\pi} e^{-9y/4} x_0^{-2} x^{-2} e^{(x_0 - x)/2} \int_0^\infty e^{-u^2 y} \frac{u \sinh(\pi u)}{(1 + 4u^2)(9 + 4u^2)} \times W_{2,iu}(x_0) W_{2,iu}(x)\, du + \frac{e^{-x}}{2} + \frac{e^{-x-2y}}{2} \frac{(2 - x)(2 - x_0)}{x_0 x}. \tag{4}$$

Here y is the dimensionless time or Compton-y parameter given by

$$y(t) \equiv n_e \sigma_T c \frac{kT_e}{m_e c^2}(t - t_0), \tag{5}$$

x is the dimensionless photon energy given by equation 2, x_0 the dimensionless photon energy at time t_0 and location r_0, and $W_{2,iu}$ are the Whittaker functions. In equation 5, n_e is the electron number density, σ_T the Thomson cross-section, c the speeds of light, k the Boltzmann constant, T_e the electron temperature, and t the time. For the full derivation of Green's function solution to the Kompaneets' equation, one can refer to Becker (2002)[2].
Using equation 4 and equation 6, the solution to the distribution function, $f(x, y)$, can be found.[2, 24]

$$f(x, y) = \int_0^\infty x_0^2 f_0(x_0) f_G(x, x_0, y) dx_0, \tag{6}$$

Here, $f_0(x)$ is the initial spectrum, and x_0 the initial energy.[2, 24]

2.3. Black body Radiation

To simplify the model, the compact object is assumed to be a black body. In a black body matter and radiation are in thermodynamical equilibrium since photons are scattered many times in an optically thick region. The model created in this paper has special units. Therefore, in this subsection, an expression for the specific intensity in the correct units for the model is obtained. It also obtains equations to calculate the new temperature needed for the feedback model.

The specific intensity of black body radiation or also called Planck radiation law is given by

$$B_\nu(T_{bb}) = \frac{2h\nu^3}{c^2} \frac{1}{e^{h\nu/kT_{bb}} - 1}. \tag{7}$$

This equation can be rewritten into terms of energy by using

$$B_\nu(T_{bb}) d\nu = B_E(T_{bb}) dE. \tag{8}$$

This will give the Planck law in terms of energy:

$$B_E(T_{bb}) = \frac{2E^3}{c^2 h^2} \frac{1}{e^{E/kT_{bb}} - 1} \frac{1}{h}. \tag{9}$$

Where $E = h\nu$. Here T_{bb} is the temperature of the black body, h the Planck constant, ν the frequency, c the speed of light, k the Boltzmann constant, and E the energy.[5, 24, 25] Redefining the energy into a dimensionless quantity x, where $x = E/kT_e$, gives an intensity of

$$B_x(T_{bb}) = \frac{2 \cdot (x \cdot kT_e)^3}{c^2 h^2} \frac{1}{e^{\frac{x * kT_e}{kT_{bb}}} - 1} \frac{1}{h}, \tag{10}$$

$$B_x[(1/2)c^2 \cdot h^3 \cdot kT_e^{-3}] = x^3 \frac{1}{e^{x/kT} - 1}. \tag{11}$$

Here $kT = \frac{kT_{bb}}{kT_e}$, where kT_e is the electron temperature. The specific intensity given in equation 11 is in the correct units for the model and is needed to calculate the feedback.
The specific intensity can be used to calculate the luminosity of the black body with

$$L = 4\pi^2 R^2 B(T_{bb}). \tag{12}$$

Where $B(T_{bb})$ is defined by

$$B(T_{bb}) = \int_0^\infty B_E(T_{bb}) dE = \int_0^\infty B_x(T_{bb}) \frac{2kT_e^4}{c^2 h^3} dx, \tag{13}$$

and R is the radius of the black body. The luminosity from equation 12 can then be used to calculate the temperature of the black body:

$$T = \sqrt[4]{\frac{L}{\sigma}}. \tag{14}$$

Here σ is the Stefan-Boltzmann constant and is defined by $\sigma = 5.670374419 \cdot 10^{-5} [erg \cdot s^{-1} \cdot K^{-4} \cdot cm^{-2}]$.[12, 18]

2.4. Quasi-periodic oscillations (QPO)

The power spectra of X-ray binaries show quasi-periodic oscillations or QPOs. These fast signals are nearly periodic and mostly in the kilohertz range of the spectrum. They are therefore often referred to as kilohertz quasi-periodic oscillations (kHz QPOs). However, these oscillations can also occur in the lower frequency part of the spectrum and are then referred to as LF QPOs (or low-frequency quasi-periodic oscillations). It is currently unknown what the origin is of these QPOs.[6] Figure 2 shows an example of an X-ray power spectrum containing QPOs.

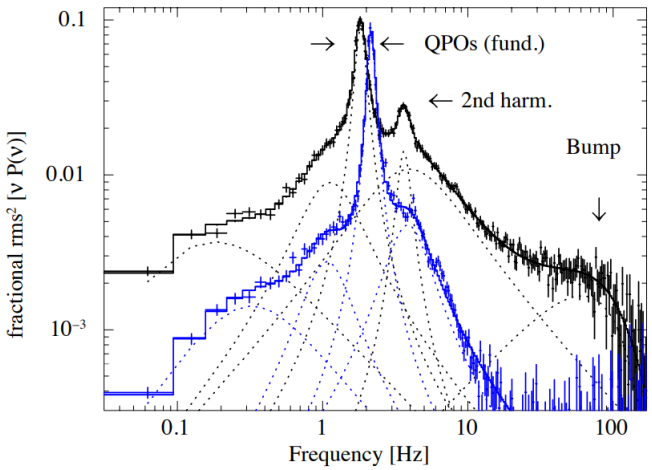

Figure 2: X-ray Fourier power spectra of GRS1915+105 with a strong fundamental QPO around 2 Hz for both the blue and black spectra. Here the dotted lines are several Lorentzian fits combined into one fit (solid lines). Taken from Mendez et al. (2022)[17].

Multiple origins of QPOs have been suggested, such as temperature oscillations in the disk or neutron star, temperature oscillations in a Comptonised region (or corona) around the disk, optical depth oscillations in the corona, matter precessing at the Lense-Thirring precession frequency (LTP) and brightness oscillations due to the rotation of bright spots on the surface of the neutron star.[11]
Models have also been created to explain the origin of QPOs. The relativistic precession model (RPM)[26] explains that the LF QPO is caused by matter precessing at the LTP. This frequency is the difference between the orbital epicyclic frequency and the vertical epicyclic frequency. The kHz QPO can be explained by it being the orbital epicyclic frequency.[11] The sonic-point beat-frequency (SPBF) model[19] explains the upper kHz QPO by it being the Keplerian frequency of the matter at the inner radius (sonic radius) around a neutron star. It also explains the lower kHz QPO to be a beat between the Keplerian frequency and the neutron star spin.[11] A beat between frequencies is the absolute value of the difference between the frequencies.[21] This beat between the Keplerian frequency and neutron star spin is also explained in the beat frequency model by Alpar & Shaham (1985)[1].
Hameury, King & Lasota (1985)[10] described that a magnetic field mechanism can produce bright spots on the surface of the neutron star. These spots rotate with the neutron spin and therefore create brightness oscillations which can be seen as QPOs.[11]
Another model about the origin of QPOs was made by Boyle, Fabian & Gilbert (1986)[4]. They were the first to suggest a Comptonising medium, also called a corona, from which the QPOs origin could be explained. They related the QPO frequencies to the optical depth of the corona, where the corona exists above the accretion disk.[11]
Lee & Miller (1998)[14], Lee, Misra & Taam (2001)[15], and Kumar & Misra (2014)[13] all proposed models with a thermal Comptonising medium where the thermodynamic properties are oscillating. These properties are the temperature and external heating rate of the corona, the electron density of the corona, and the temperature of the soft photon source that provides the seed photons for Comptonization. Lee & Miller (1998)[14] were able to create a model to simulate the rms and time lags due to Comptonization of a seed photon source in a homogeneous and spherically symmetric corona.[11]
In the model of Lee, Misra & Taam (2001)[15] it is assumed that the temperature oscillation of the seed photon source is delayed due to the oscillation in the corona temperature. This delay happens through feedback, where a part of the Comptonised photons in the corona fall back into the source. These photons will heat the source creating a temperature oscillation.[11]

3. Method and Results

This section will describe the method and results of the research. To be able to implement the feedback in the Python program, the code that has already been created in Roomer (2021)[24] needs to be checked. This will be done first in section 3.1. When the code has proven to work, the feedback will be implemented. Section 3.2 will discuss how the code with feedback works and the results that follow. The fundamental QPO in the power spectra will be fitted with a Lorentzian in section 3.3.
The model for injection rate oscillations, temperature oscillations, and the model containing feedback can be found on the Gitlab page of the author.[23]

3.1. Testing code

First, to be able to implement the feedback, it is important to check if the model that has been created in the previous project still creates the same results as obtained in Roomer (2021)[24]. For a full description of this model, one can refer to Roomer (2021)[24]. The model can be checked by implementing the same values as previously done and checking the light curves

and power spectra with the plots shown in Roomer (2021)[24]. Both the injection rate oscillations and temperature oscillations will be checked for an angular frequency of $\omega = 2\pi$ rad/s, a black body temperature of $kT = 0.1[kT_e^{-1}]$ and a mean value of the Compton-y parameter of $\tilde{y} = 1.0$, as was also done in Roomer (2021)[24].
First, the injection rate oscillations will be checked. Here the time-dependent escaping photon distribution is calculated using

$$B_x(x,t) = \int_0^{t/t_{esc}} \dot{N}_0 \left(1 + A\sin\left(wt_0\right)\right) e^{-\frac{t-t_0}{t_{esc}}} x^2 f\left(x, x_0, \tilde{y}\left(\frac{t-t_0}{t_{esc}}\right), kT\right) dt_0. \tag{15}$$

Where $f\left(x, x_0, \tilde{y}\left(\frac{t-t_0}{t_{esc}}\right), kT\right)$ is given by equation 6 with a black body initial spectrum for f_0. Here $B_x(x,t) = \dot{N}_x(x,t)$ from equation (25) and (31) of Roomer (2021)[24].
The middle panels in Figure 18 from Roomer (2021)[24] for the light curve and Figure 19 from Roomer (2021)[24] for the power spectrum were replicated. Figure 3 and Figure 4 show the results obtained.

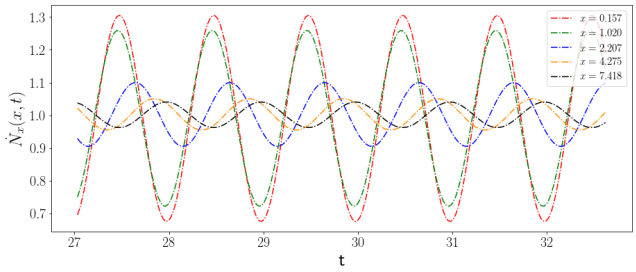

Figure 3: Light curve obtained for injection rate oscillations to compare with Figure 18 from Roomer (2021)[24]. Here $\omega = 2\pi$ rad/s, $kT = 0.1[kT_e^{-1}]$, $\tilde{y} = 1.0$.

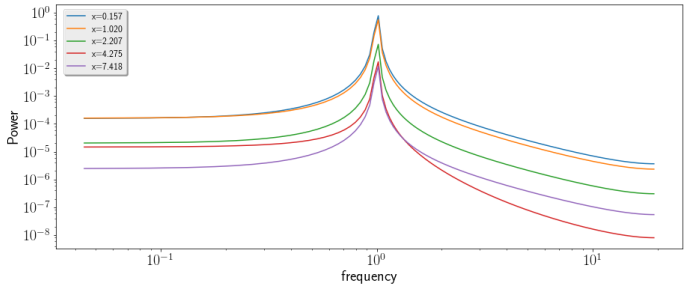

Figure 4: Power spectrum for injection rate oscillations to compare with Figure 19 from Roomer (2021)[24]. Here $\omega = 2\pi$ rad/s, $kT = 0.1[kT_e^{-1}]$, $\tilde{y} = 1.0$.

This result is the same as the light curve and power spectrum obtained for these values in Roomer (2021)[24].
Next the temperature oscillations need to be plotted. The escaping photon distribution for these oscillations is calculated using

$$B_x(x,t) = \int_0^{t/t_{esc}} \dot{N}_0 e^{-\frac{t-t_0}{t_{esc}}} x^2 f\left(x, x_0, \tilde{y}\left(\frac{t-t_0}{t_{esc}}\right), \left(1 + A\sin\left(wt_0\right)\right) kT\right) dt_0. \tag{16}$$

Where $f\left(x, x_0, \tilde{y}\left(\frac{t-t_0}{t_{esc}}\right), \left(1 + A\sin\left(wt_0\right)\right) kT\right)$ is given by equation 6 with a black body initial spectrum for f_0 and $B_x(x,t) = \dot{N}_x(x,t)$ from equation (25) and (33) of Roomer (2021)[24].
The results are shown in Figure 5 for the light curve and Figure 6 for the power spectrum. These will be compared with the middle panels of Figure 20 and Figure 21 from Roomer (2021)[24].

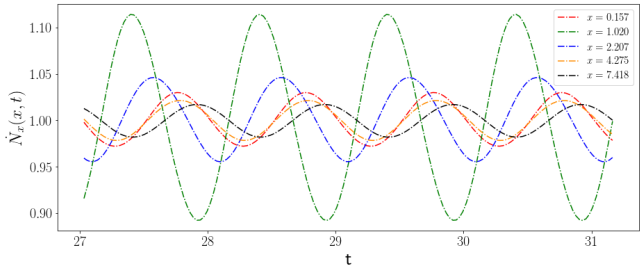

Figure 5: Light curve obtained for temperature oscillations to compare with Figure 20 from Roomer (2021)[24]. Here $\omega = 2\pi$ rad/s, $kT = 0.1[kT_e^{-1}]$, $\tilde{y} = 1.0$.

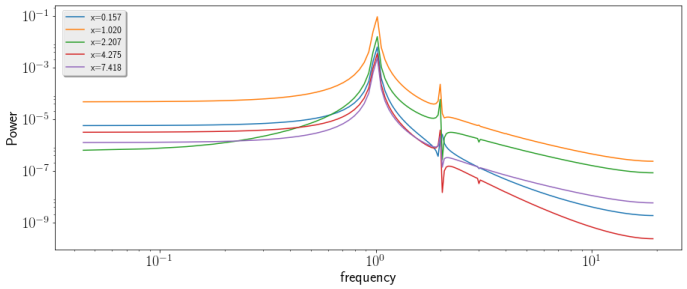

Figure 6: Power spectrum for temperature oscillations to compare with Figure 21 from Roomer (2021)[24]. Here $\omega = 2\pi$ rad/s, $kT = 0.1[kT_e^{-1}]$, $\tilde{y} = 1.0$.

These figures are identical to the ones from Roomer (2021)[24].
However, the values that were used for the variables were non-realistic. Therefore, it is necessary to check whether the model will also work when implementing values that are based on parameters obtained from observations.
The code is tested with these more realistic values for both the injection rate oscillations and the temperature oscillations. Figure 7 and Figure 8 show respectively the light curve and power spectrum for injection rate oscillations with realistic values. The power spectrum can be created by performing a Fast Fourier Transform (FFT) on the light curves.

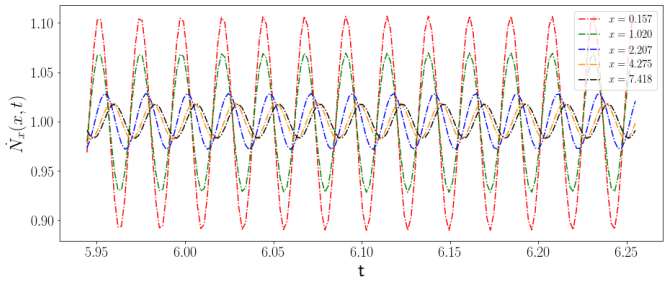

Figure 7: Light curve for injection rate oscillations with more realistic values. Normalized to the mean value. Here $\tilde{y} = 2.0967$, $\omega = \frac{2\pi}{0.0233}$ rad/s, $kT = 0.1[kT_e^{-1}]$ and $A = 0.2$. Where $t_{esc} = 0.0233$ s.

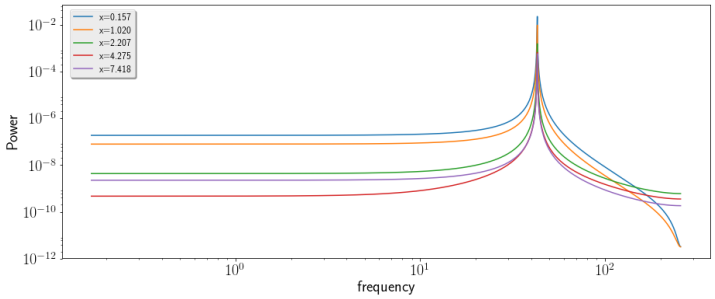

Figure 8: Power spectrum for injection rate oscillations for more realistic values. Here $\tilde{y} = 2.0967$, $\omega = \frac{2\pi}{0.0233}$ rad/s, $kT = 0.1[kT_e^{-1}]$ and $A = 0.2$. Where $t_{esc} = 0.0233$ s.

As can be seen in Figure 7, the light curves show phase lags and the amplitude decreases with increasing energy. These phase lags are caused by energy gain or also called up-scattering of the photons since the corona has a higher temperature than the black body. The amplitude changes are caused by Comptonization as was established already in Roomer (2021)[24].
As expected, the height of the peaks in the power spectrum in Figure 8 decreases with increasing energy. This is due to the amplitude of the light curves decreasing.
Figure 9 and Figure 10 show the light curves and power spectrum for temperature oscillations with realistic values.

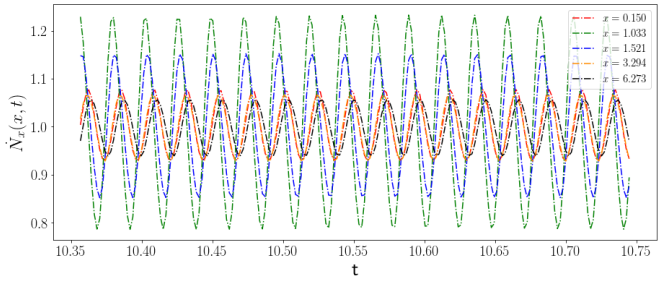

Figure 9: Light curve for temperature oscillations with more realistic values. Normalized to the mean value. Here $\tilde{y} = 2.0967$, $\omega = \frac{2\pi}{0.0233}$ rad/s, $kT = 0.1[kT_e^{-1}]$ and $A = 0.2$. Where $t_{esc} = 0.0233$ s.

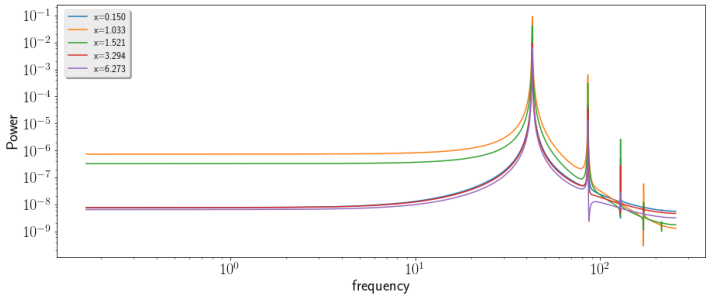

Figure 10: Power spectrum for temperature oscillations for more realistic values. Here $\tilde{y} = 2.0967$, $\omega = \frac{2\pi}{0.0233}$ rad/s, $kT = 0.1[kT_e^{-1}]$ and $A = 0.2$. Where $t_{esc} = 0.0233$ s.

The amplitude of the light curves decreases with increasing energy, as expected. However, this is not the case for $x = 0.150$. To better understand this behavior the amplitude as a function of energy is plotted in Figure 11.

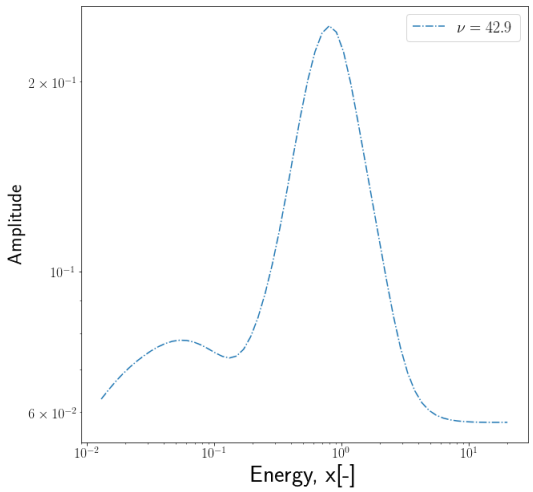

Figure 11: Amplitude versus energy for temperature oscillations with a frequency of $\nu = \frac{1}{0.0233}$ Hz.

Looking at Figure 11, the curve has a well-defined shape. This explains the behavior seen in Figure 9.

The phase lags in Figure 9 also increase with increasing energy as expected. This is due to the same reason as explained above.
Due to the temperature oscillations being proportional to

$$\frac{1}{e^{x\frac{kT_e}{kT(1+\sin(\omega t))}}} - 1,$$

the power spectrum in Figure 10 shows not only a fundamental harmonic but also higher harmonics. Again, the height of the spectra decreases with increasing energy, due to the amplitude changes in the light curve in Figure 9.

3.2. Feedback model

It is now known that the code for the injection rate oscillations and temperature oscillations works properly. Next, the feedback can be implemented in the model. The way this is done is as follows. To calculate the new temperature, the luminosity needs to be known (eq. 14). This luminosity can be calculated using equation 12 and equation 13. The values of B_x are obtained from the model. The values of B_x at time $t-1$ ($B_{x,-1}$) can then be used to calculate the new B_x with

$$B_x = B_{x,0} + factor * B_{x,-1}. \tag{17}$$

Here $B_{x,0}$ is the specific intensity of the initial black body at a temperature of kT that is initially specified and the factor indicates the percentage of photons that fall back into the black body. This B_x can be used in equation 13 to calculate $B(T)$ and ultimately calculate the new temperature at time t. This new temperature will be implemented in the model for the next time step. A flowchart of the process can be found in Figure 20 in Appendix A. The Python code for the model can be found on the Gitlab page of the author.[23]
Using the model, the power density spectra (PDS) can be obtained. This can be used to study the behavior of the PDS and specifically the behavior of the width of the QPO peaks with changing angular frequency. The spectra have been created for five different angular frequencies, where one frequency is the harmonic frequency of $\nu_{esc} = 1/t_{esc}$. The power spectra for the five different angular frequencies can be found in Figure 12.

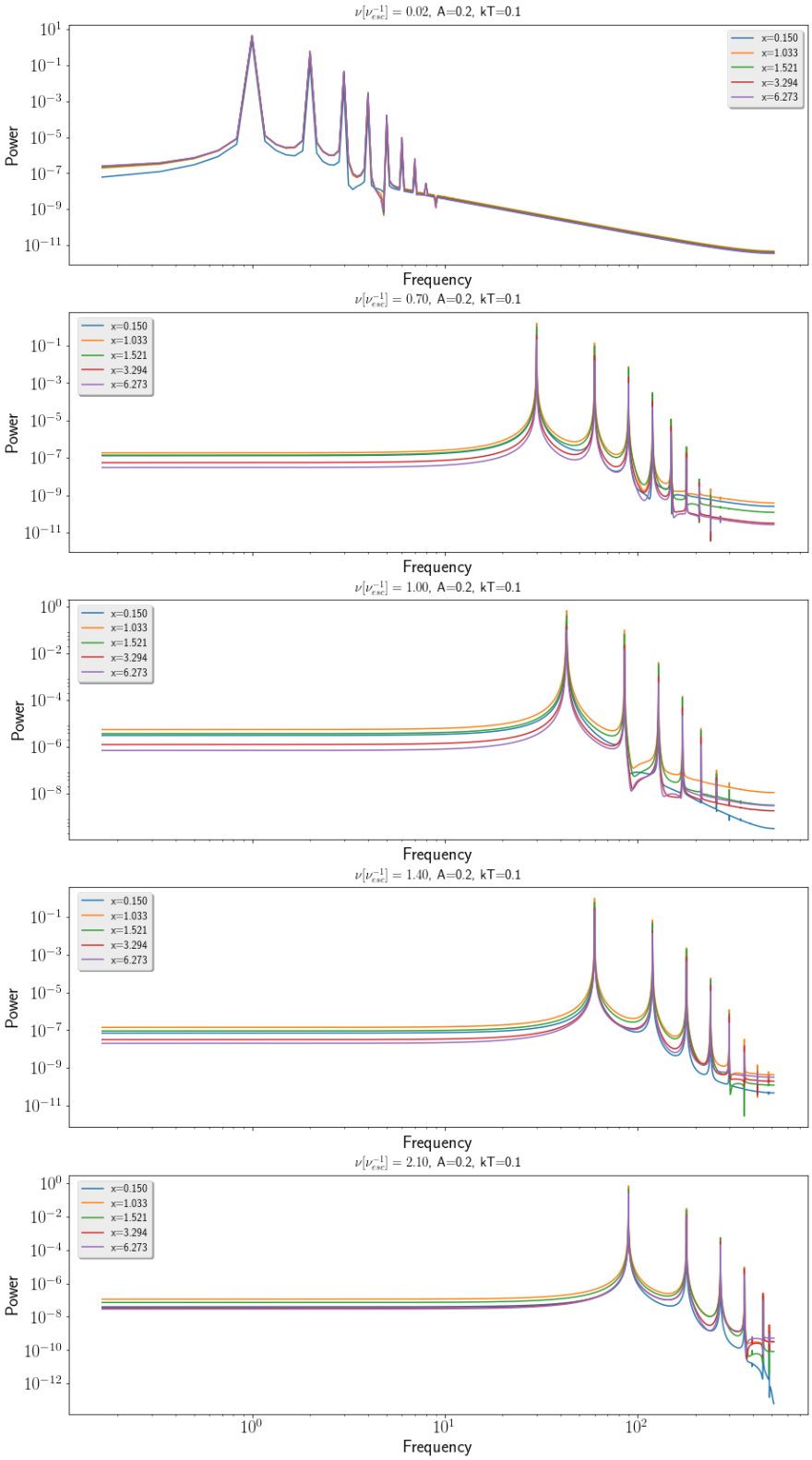

Figure 12: Power spectrum for different frequencies in units of the escape frequency $\nu_{esc} = 1/t_{esc}$. From top to bottom the frequencies are $\nu = 1$ Hz, $\nu = 30$ Hz, $\nu = 1/t_{esc} = 42.9$ Hz, $\nu = 60$ Hz, $\nu = 90$ Hz. In all panels $\tilde{y} = 2.0967$, $kT = 0.1[kT_e^{-1}]$, $t_{esc} = 0.0233$ s, $A = 0.2$.

Using these power spectra the phase lags for the fundamental harmonic can be determined and plotted. This is shown in Figure 13.

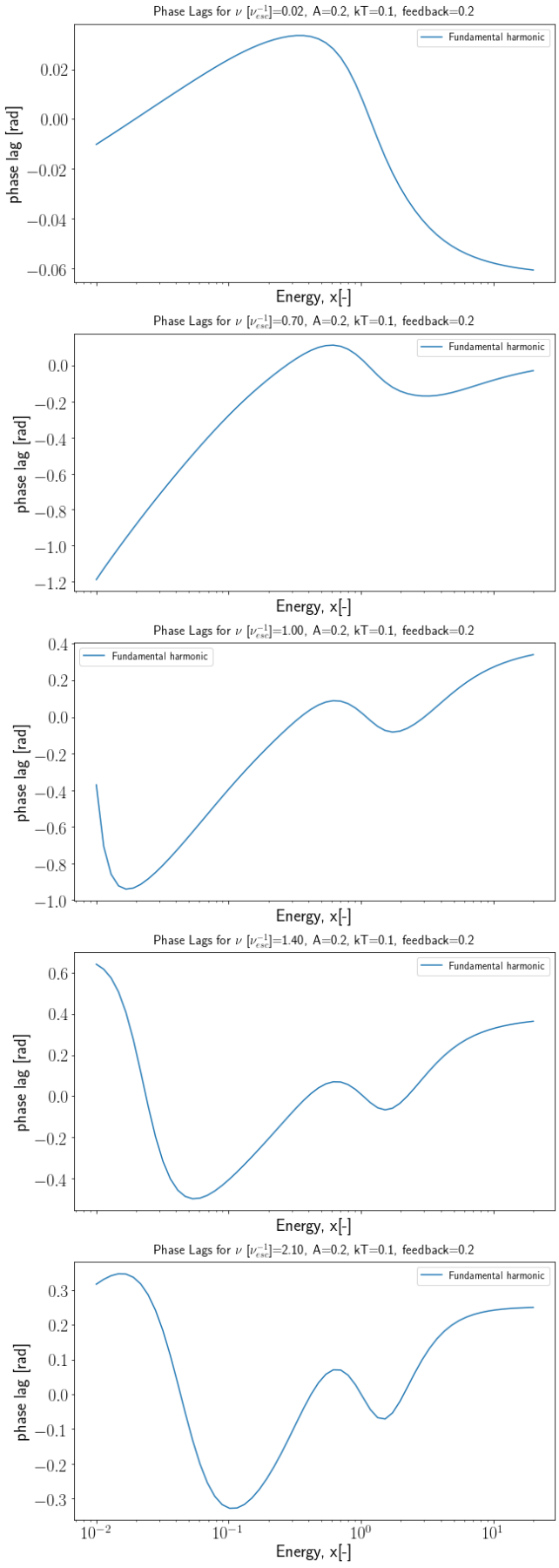

Figure 13: Phase lags of fundamental harmonic for different frequencies in units of the escape frequency $\nu_{esc} = 1/t_{esc}$. From top to bottom the frequencies are $\nu = 1$ Hz, $\nu = 30$ Hz, $\nu = 1/t_{esc} = 42.9$ Hz, $\nu = 60$ Hz, $\nu = 90$ Hz. In all panels $\tilde{y} = 2.0967$, $kT = 0.1[kT_e^{-1}]$, $t_{esc} = 0.0233$ s, $A = 0.2$.

In this model the optical depth $\tau = 1$. This indicates that there are not many scatterings and the lags are therefore small. For frequencies below the escape frequency ($\nu < \nu_{esc} = 1/t_{esc}$) the lags increase for low energies. This increase is due to up-scattering in the corona. Since the energy of the photons is below the energy of the corona the photons will gain energy when colliding with an electron in the corona. The higher this energy the longer the delay of these photons and thus the phase lags increase. When the energy of the photons reaches approximately the energy of the corona and above the lags start to decrease. Here, the photons lose energy or down-scatter since they have a higher energy than the electrons in the corona. When they collide with these electrons they lose energy. It is expected that the value at which the transition from up to down-scattering occurs is around a value of $x = 1$, since here the temperature of the black body would be equal to that of the corona. However, looking at Figure 13, this turning point does not occur at $x = 1$. The bottom two plots do not even show a distinct shape with one up- and one down-scattering part. It is currently unknown why this is the case and needs to be further investigated.

The phase lags start to show different behavior when they reach the escape frequency and above. As can be seen from the bottom two plots in Figure 13 the lags show a big "u-shape" at low energies and a smaller "u-shape" at higher energies. Here the variations are faster than the escape time of the photons and thus the corona has less time to reach a new equilibrium state, which might explain the behavior seen. The energy at which the minimum of this low-energy "u-shape" is found increases with increasing feedback. To better explain this behavior the root mean square or rms versus energy is plotted in figure 14.

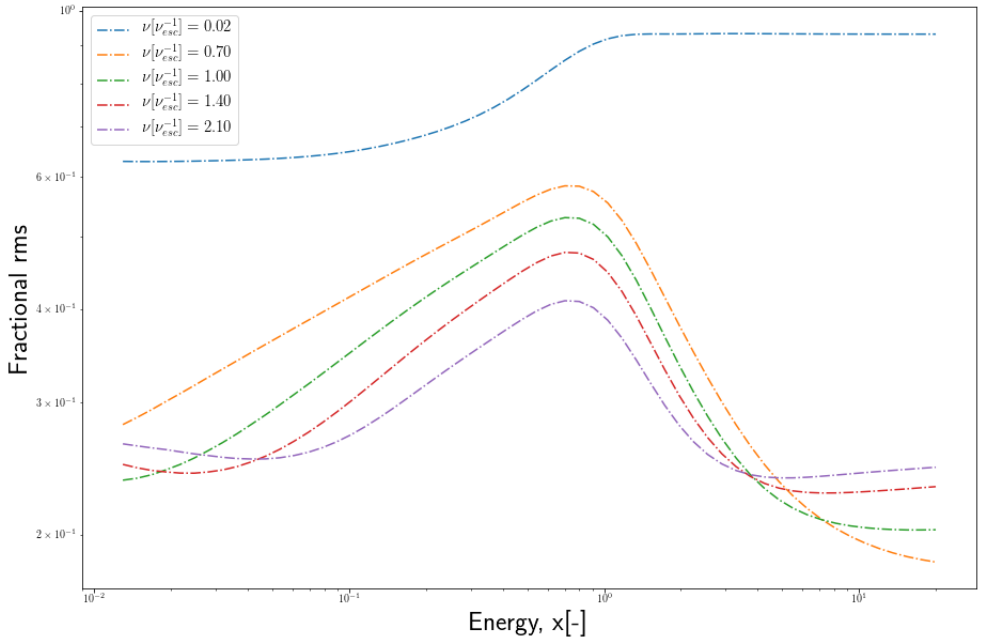

Figure 14: Root Mean Square of light curves for each frequency value.

The lags for $\nu = 1.4[\nu_{esc}^{-1}]$, $\nu = 2.1[\nu_{esc}^{-1}]$, and a small part of the lags of $\nu = 1.0[\nu_{esc}^{-1}]$ have a very steep slope at low energies. This steep slope can be explained by the rms values having a minimum around those energies, as can be seen in Figure 14. This minimum shifts to the right with increasing frequency, and therefore so does the slope in Figure 13.

To see the influence of the feedback on the lags, the lags for three different feedback factors are plotted in Figure 15. Here, the frequency is constant at a value of $\nu = 1$ Hz, and the

mean value of the Compton-y parameter, the temperature, and the amplitude of the oscillations are also kept constant.

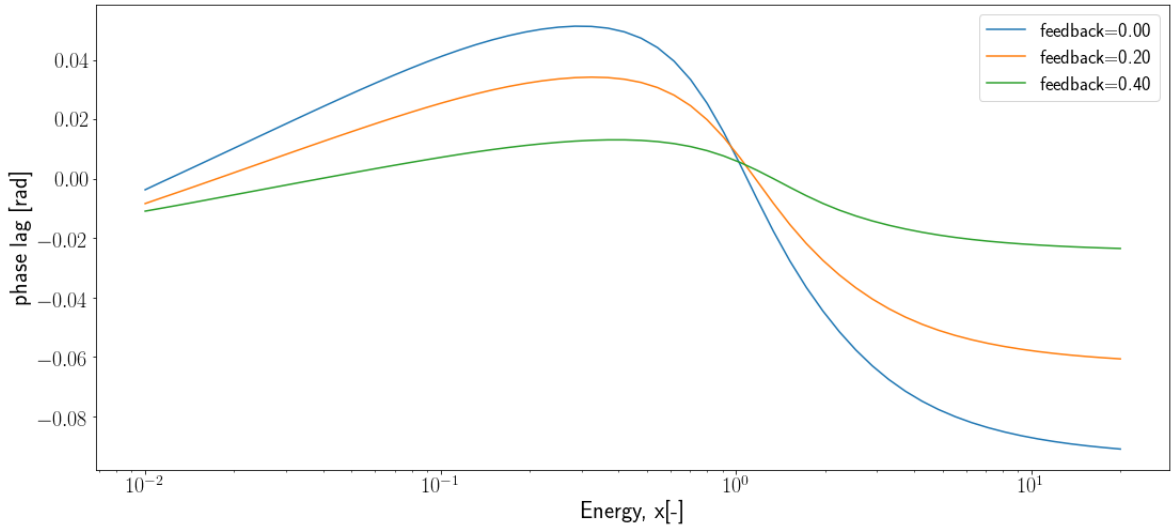

Figure 15: Phase lags of fundamental harmonic for $\nu = 1$ Hz $= 0.0233[\nu_{esc}^{-1}]$ for different feedback factors of 0.0, 0.2 and 0.4. Here $\tilde{y} = 2.0967$, $kT = 0.1[kT_e^{-1}]$, $t_{esc} = 0.0233$ s, $A = 0.2$.

The curve for the lags flatten out with increasing feedback but remain to have a similar shape. The soft lags here increase, while the hard lags do not change a lot with changing frequency, causing the lags to soften for a higher feedback factor. This effect is also seen by Candela(2022)[3]. Some of the photons that were up-scattered return to the black body when there is feedback. Where the number of these photons returning increases with increasing feedback. These photons are reprocessed and thermalized in the black body, leading to low-energy photons escaping the corona. This increases the soft lags.[3] This might be the reason for the softening of the lags with increasing feedback, but more research is necessary to confirm this. The peaks in Figure 15 shift slightly to the right with increasing feedback. It is currently unknown why this behavior is seen and is a topic for further research.
The lags are positive (or also called hard lags) for the low-energy range, where the lags become soft at higher energies. This can be explained by the hard photons undergoing more scattering at lower energies than low-energy photons. Vice versa, the soft photons undergo more scattering at higher energies than the hard photons, causing the lags to become negative. This explains the transition from positive to negative lags around $x = 1$, since here the temperature of the corona is equal to the temperature of the black body. Figure 15 can be compared with the bottom left panel of Figure 2 in Candela (2022)[3]. Here it is also seen that the lags have a pivot point at a certain energy value. However, this is a different model with different values for the parameters and therefore the exact values on the axes cannot be compared.
To better explain the behavior of the lags in Figure 15 the rms per energy is plotted in Figure 16.

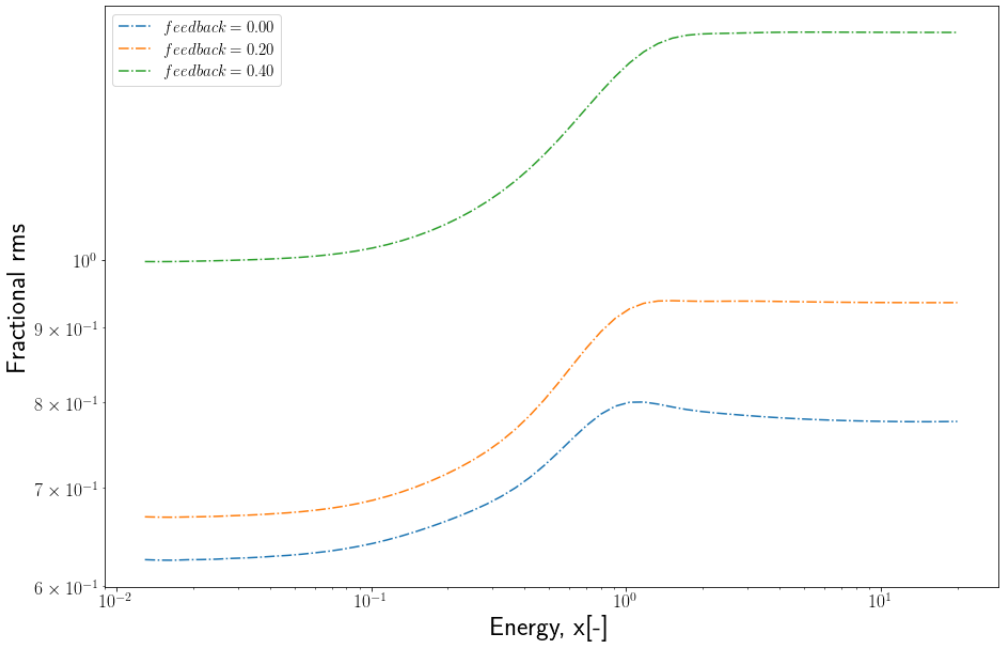

Figure 16: Root Mean Square of light curves for each feedback factor. The frequency is kept constant at $\nu = 1$ Hz $= 0.02[\nu_{esc}^{-1}]$. Here $\tilde{y} = 2.0967$, $kT = 0.1[kT_e^{-1}]$, $t_{esc} = 0.0233$ s, $A = 0.2$.

Here it is seen that the rms increase with increasing feedback factor. This explains the softening of the lags seen in Figure 15. Figure 16 also shows that when the energy reaches a value of $x = 1$, i.e. the black body temperature reaches the corona temperature, the rms values become relatively constant. This explains the flattening of the curves seen at high energies in Figure 15.

3.3. Lorentzian fit

To measure the width of the QPOs a Lorentzian is fitted to the PDS. Since the PDS consists of multiple QPOs, multiple Lorentzians are fitted and combined to form one fit. This is shown in Figure 17 for both the combined fit and the individual components of the fit for a frequency of $\nu = 60$ Hz.

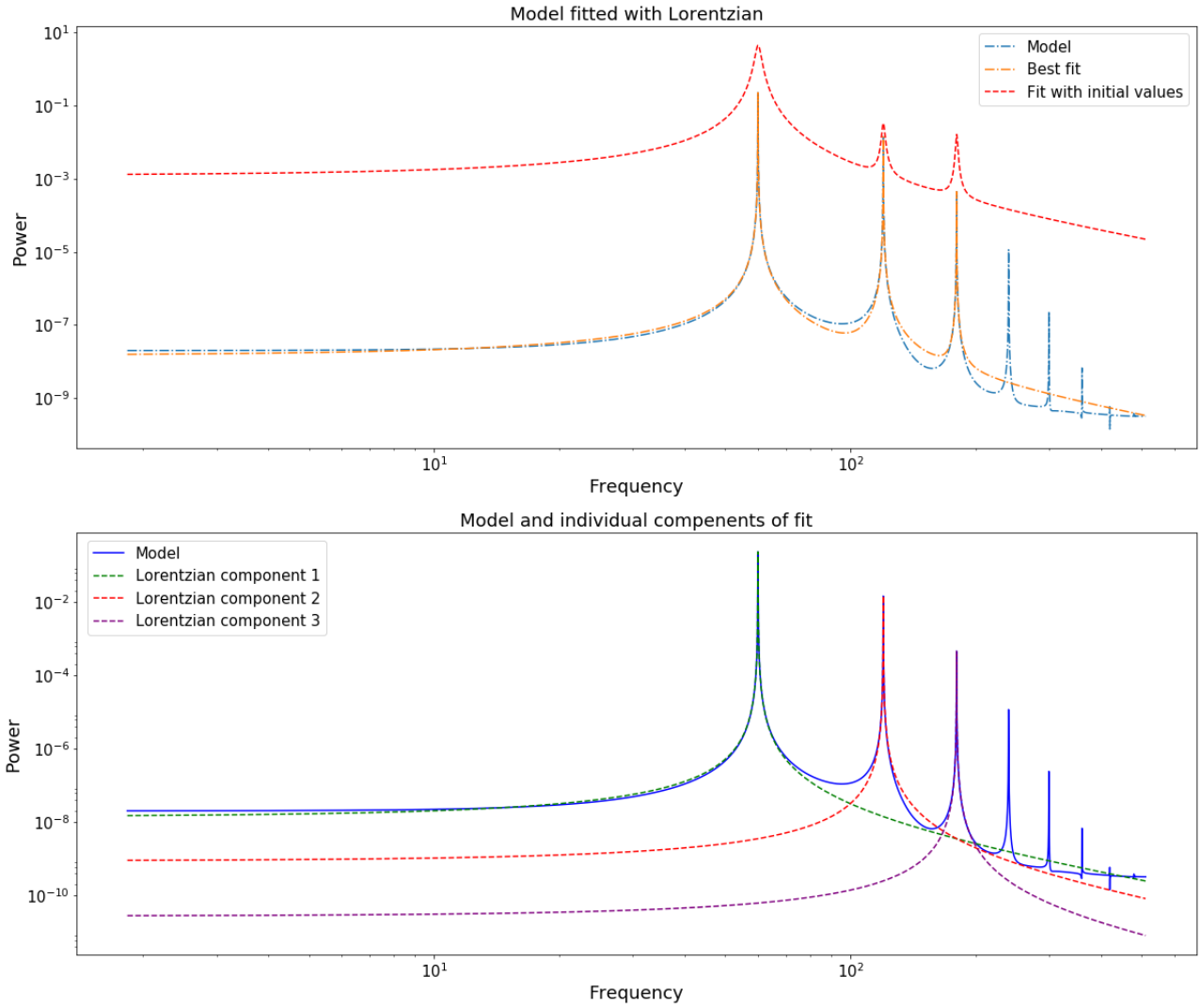

Figure 17: In the top panel the fit of the Lorentzian is shown and the bottom panel shows the components of the individual Lorentz fits used to make the total fit for the PDS. Here $\nu = 60$ Hz, $\tilde{y} = 2.0967$, $A = 0.2$, $kT = 0.1[kT_e^{-1}]$ and $t_{esc} = 0.0233$ s.

Using this model the width of the fundamental QPO can be determined. In the case of $\nu =$ 60Hz the Full Width Half Maximum (FWHM) is determined to be FWHM$= 0.0008 \pm 0.0007$ Hz.

4. Discussion

There are some points that can be discussed as to why some things were done or why certain results are useful. This discussion is divided into two parts: One that discusses the theoretical model and another that discusses the physics behind it.

4.1. Theoretical model

Since the model runs for a large number of points, it is important that the code is as fast as can be. However, this is an analytic model and therefore takes a longer time for the calculations than if it were a numerical model. The basic limitations of the model are discussed in chapter 4.1 of Roomer (2021)[24]. Nonetheless, the new feedback model has oscillations combined with the feedback and needs a large number of points for the time to avoid aliasing. This large number of time values causes the run-time to increase.
The main limitation of this model is the constant corona. Here the properties of the corona do not change with time. The electron temperature of the electrons in the corona, the size of the corona, and the optical depth are all assumed constant, whereas in a more accurate case these would vary. The corona is also assumed spherical and homogeneous, which is a simplification of the model and does not resemble reality.
This model is also not practical to fit to data, but only to compare it with data. When fitting to data the parameters in the model need to change individually as free parameters to obtain the best fit. Due to the long run time of the model, this is not possible on a realistic time scale. The feedback model also goes to higher energies than currently possible in observations. The satellites available will only go to an energy of approximately 30 keV maximum. This is approximately the value of the electrons in the corona (kT_e). Since the model created goes to energies above those values, we cannot compare the whole range of energies with data. This is also one of the reasons it is currently unknown why the peak of the lags for frequencies below the escape frequency is not at a value of $x = 1$.
The feedback in the model is instantaneous. At each time value, a percentage of the photons injected one time step prior are going back to the black body instantaneously. In a more realistic case, these feedback photons are a distribution and some photons take longer to fall back into the black body than others. Therefore a photon that was emitted into the corona might also fall back into the black body two or more time steps later, which is not implemented in this model.
Finally, Figure 18 shows the fractional rms and phase lags of black hole transient MAXI J1348-630 obtained from observations.

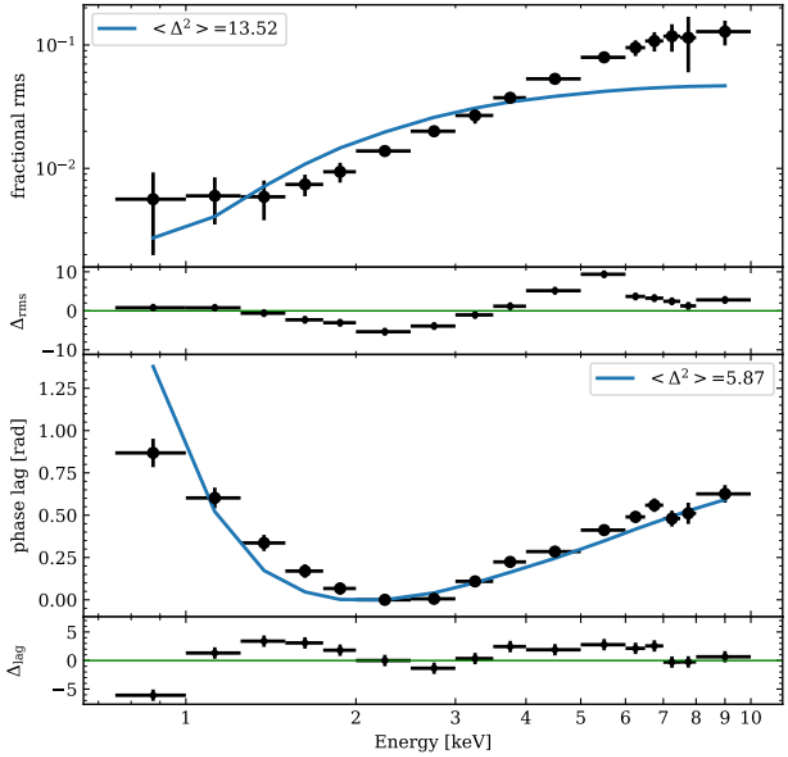

Figure 18: Fractional rms (top panel) and phase lags (lower panel) of the QPO from the black hole transient MAXI J1348–630. The individual points represent the data and the solid lines a model fitted by Garcia et al. (2020)[9]. Taken from Garcia et al. (2020)[9]

In Figure 18, the black points represent the data. Since these are from observations, the energy values are low for the reason explained above. The phase lags in the bottom panel can be compared with the phase lags in Figure 13. However, this can only be compared for the left side of the figure, since the energies in Figure 18 do not go higher than 10 keV. Garcia (2020)[9] calculated an electron temperature of $kT_e = 20$ keV, by fitting a model to the data (blue line). This makes it possible to calculate the energy values in the units for the model created in this paper. This will give energies between approximately $x = 0.03$ and $x = 0.5$. Figure 18 can be better compared to Figure 13 when it is selected for the same energy range. This is done for the bottom two panels of Figure 13 and shown in Figure 19.

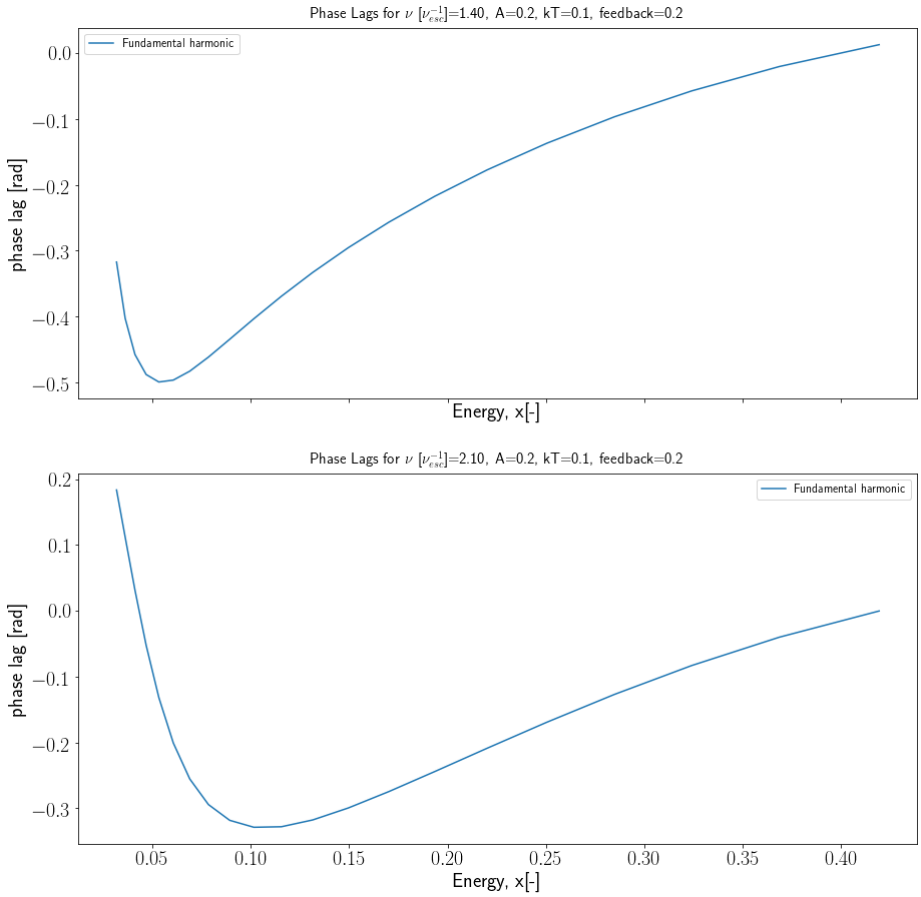

Figure 19: Phase lags obtained with model cropped to the energy range of Figure 18. Here the phase lags for the frequency of $\nu[\nu_{esc}^{-1}] = 1.4$ and $\nu[\nu_{esc}^{-1}] = 2.1$ are plotted.

It can be seen that the shape of the lags shows quite a resemblance, especially for the lower panel of Figure 19. However, the frequency of the QPO in Figure 18 is $\nu = 4.45$ Hz, whereas the frequencies in the lags from the model shown in Figure 19 are $\nu = 60$ Hz and $\nu = 90$ Hz respectively. The model created in this paper is still a preliminary model containing many simplifications. Therefore, the exact values of the parameters may differ. For example, in Figure 18 the source temperature is obtained with the best fit and estimated at approximately $kT_{bb} = 0.2$ keV.[9] This is equal to a $kT = 0.01$, in the units of this model. The lags obtained in Figure 13 are all for a value of $kT = 0.1$. These differences do not imply that the model is not useful. As mentioned, the shapes are very similar and indicate that the model created has the potential to give a better understanding of the observations.
The rms from the observations of MAXI J1348-630 in Figure 18 can also be compared with the rms from the model shown in Figure 14. Here it is seen that the shape of the rms from the data also has a resemblance to the shape of the rms shown in Figure 14 for the frequency of $\nu = 1$ Hz $= 0.02[\nu_{esc}^{-1}]$.

4.2. Physics

In this section, the physics and results of the model will be discussed. It is divided into two parts. First, the model with feedback will be discussed and in 4.2.2 the Lorentzian fit shown in section 3.3 is discussed.

4.2.1. Feedback model

As can be seen in Figure 12 the peaks of the PDS move to the right with increasing angular frequency. This is expected since the fundamental QPO will be at the frequency implemented in the model and this value increases with each plot, causing the peaks to shift to the right. The peak of the first PDS where $\nu = 1$ Hz looks broader than the other ones. However, this is due to the fact that the peak is shifted more to the left on the x-axis and the axis has a log scale.
The peaks of the phase lags for different values of the feedback factor shift to the right with increasing feedback, as can be seen in Figure 15. However, it is unknown why this happens and it is necessary to further look into this behavior.

4.2.2. Lorentzian fit

The value determined for the FWHM of the fundamental QPO at $\nu = 60$ Hz is very small and close to zero. The reason for this is that the light curves are quasi-sinusoidal and the amplitude does not change much over time for each energy value. The oscillations do not decay and remain roughly the same over time. Therefore the FFT will create peaks that are close to a delta function at the frequency resolution and do not resemble a Lorentzian. This makes it not useful to measure the width of the peaks since they will always go to a value of zero. This is the case at each frequency and therefore it is decided that it is not necessary to analyze the widths of the QPOs of the other PDS.

5. Conclusion

An analytic model to study the radiative and thermodynamical properties of a corona around a compact object including feedback has been created. This model adds a fraction of feedback from the corona back to the black body and calculates the evolution in energy space of a photon distribution in a spherically and homogeneous corona. It can be used to plot the spectra, light curves, power density spectra (PDS), phase lags, and rms of the escaping photons to compare with observations.

One of the goals of this project was to analyze the behavior of the widths of the QPO peaks in the PDS as a function of frequency. However, it was found that the peaks of the QPOs resembled a delta function and could therefore not be used to measure the width changes.

In the end, three models have been created, separated over two projects. The first two models do not contain feedback but only have either temperature oscillations or injection rate oscillations. The third model contains feedback from the corona back to the black body and also contains temperature oscillations. All models can be found on the Gitlab page of the author, including a file to plot the spectra, light curves, PDS, phase lags, and rms. It also contains a program to calculate the parameters of the model in the correct units of the model given parameters in cgs units.[23]

6. Recommendations

In order to quantitatively measure the width of the peaks at different frequencies, the amplitude of the light curve needs to change. Therefore the oscillations need more than a sinusoidal oscillation. This can be done by for example multiplying an exponential function with the oscillations of the temperature. This exponential can be a function of the optical depth. Using this function the oscillations will slowly damp. Implementing random shots can keep the

oscillations going. However, it has not been proven that this works and therefore needs to be researched further.

7. Acknowledgments

This project was supervised by Prof. Dr. Mariano Mendez. I would like to thank him for giving me such an interesting project and giving me the opportunity not to only do my university bachelor research but also my graduation internship at the university of applied sciences. I have learned more about this field of research and got to improve my Python skills for which I am grateful.
I would also like to thank Dr. Federico Garcia for helping me during this project and Valentina Peirano for taking the time to help me with Python when I had trouble finding the problem.

References

[1] M. A. Alpar and J. Shaham. GX 5-1: a Possible Millisecond Period Neutron Star? *IAU Cirulars*, 4046:2, March 1985.

[2] P. A. Becker. Exact solution for the green's function describing time-dependent thermal comptonization. *Monthly Notices of the Royal Astronomical Society*, 343(1):215–240, Jul 2003.

[3] Candela Bellavita, Federico García, Mariano Méndez, and Konstantinos Karpouzas. vkompth: A variable comptonisation model for low-frequency quasi-periodic oscillations in black-hole x-ray binaries, 2022.

[4] C. B. Boyle, A. C. Fabian, and P. W. Guilbert. Quasi-periodic oscillations from accretion disk coronas. *Nature*, 319(6055):648–649, February 1986.

[5] Hale Bradt. *Astrophysics processes: the physics of astronomical phenomena.* Cambridge Univ. Press, 2014.

[6] Max Camenzind. *Compact objects in astrophysics: white dwarfs, neutron stars and black holes.* Springer, 2007.

[7] Thierry J.-L. Courvoisier. *High energy astrophysics an introduction.* Springer, 2013.

[8] Matt DeCross, Christopher Williams, Sameer Kallasa, Deeponjit Bose, Josh Silverman, Jimin Khim, and Andrew Hayes. Green's functions in physics, Dec 2020.

[9] Federico García, Mariano Méndez, Konstantinos Karpouzas, Tomaso Belloni, Liang Zhang, and Diego Altamirano. A two-component comptonization model for the type-b qpo in maxi j1348-630. *Monthly Notices of the Royal Astronomical Society*, 501(3):3173–3182, March 2021.

[10] J. M. Hameury, A.R. King, and J. P. Lasota. A model for quasi-periodic oscillations in low-mass X-ray binaries. *Nature*, 317(6038):597–599, October 1985.

[11] Konstantinos Karpouzas. *Modelling of Comptonisation in low-mass X-ray binaries in the presence of fast variability.* PhD thesis, University of Groningen, 2021.

[12] Kevin krisciunas. How to integrate planck's function.

[13] Nagendra Kumar and Ranjeev Misra. Energy dependent time delays of kHz oscillations due to thermal Comptonization. *Monthly Notices of the Royal Astronomical Society*, 445(3):2818–2824, 10 2014.

[14] Hyong C. Lee and Guy S. Miller. Comptonization and QPO origins in accreting neutron star systems. *Monthly Notices of the Royal Astronomical Society*, 299(2):479–487, September 1998.

[15] Hyong C. Lee, R. Misra, and Ronald E. Taam. A Compton Upscattering Model for Soft Lags in the Lower Kilohertz Quasi-periodic Oscillation in 4U 1608-52. *Astrophysical Journal, Letters*, 549(2):L229–L232, March 2001.

[16] Mariano Méndez and Tomaso M. Belloni. High-frequency variability in neutron-star low-mass x-ray binaries. In *Timing Neutron Stars: Pulsations, Oscillations and Explosions*, pages 263–331. Springer Berlin Heidelberg, oct 2020.

[17] Mariano Méndez, Konstantinos Karpouzas, Federico García, Liang Zhang, Yuexin Zhang, Tomaso M. Belloni, and Diego Altamirano. Coupling between the accreting corona and the relativistic jet in the microquasar GRS 1915+105. *Nature Astronomy*, 6(5):577–583, mar 2022.

[18] Chris Mihos. Blackbody radiation;, Sep 2002.

[19] M. Coleman Miller and Frederick K. Lamb. Bounds on the compactness of neutron stars from brightness oscillations during x-ray bursts. *The Astrophysical Journal*, 499(1):L37–L40, may 1998.

[20] J.D. Myers. X-ray binary stars - introduction, 2014.

[21] Carl R. (Rod) Nave. Beats.

[22] Michael A. Nowak, Brian A. Vaughan, Jorn Wilms, James B. Dove, and Mitchell C. Begelman. Rossi x-ray timing ExplorerObservation of cygnus x-1. II. timing analysis. *The Astrophysical Journal*, 510(2):874–891, jan 1999.

[23] J. Roomer. An analytic model to study the radiative and thermodynamic properties of a corona around a compact object. `https://gitlab.astro.rug.nl/roomer/an-analytic-model-to-study-the-radiative-and-thermodynamical-properties-of-a-corona-ar` `git`, 2022.

[24] Jesse Roomer. An analytic model to study the radiative and thermodynamical properties of a corona around a compact object. Graduation thesis Engineering Physics, January 2021.

[25] George B. Rybicki and Alan P. Lightman. *Radiative processes in astrophysics*. WILEY-VCH, 2004.

[26] Luigi Stella and Mario Vietri. Lense-thirring precession and quasi-periodic oscillations in low-mass x-ray binaries. *The Astrophysical Journal*, 492(1):L59–L62, jan 1998.

A. Flowchart of Python code

A.1. Flowchart for the code to obtain the time-dependent escaping photon distribution with feedback

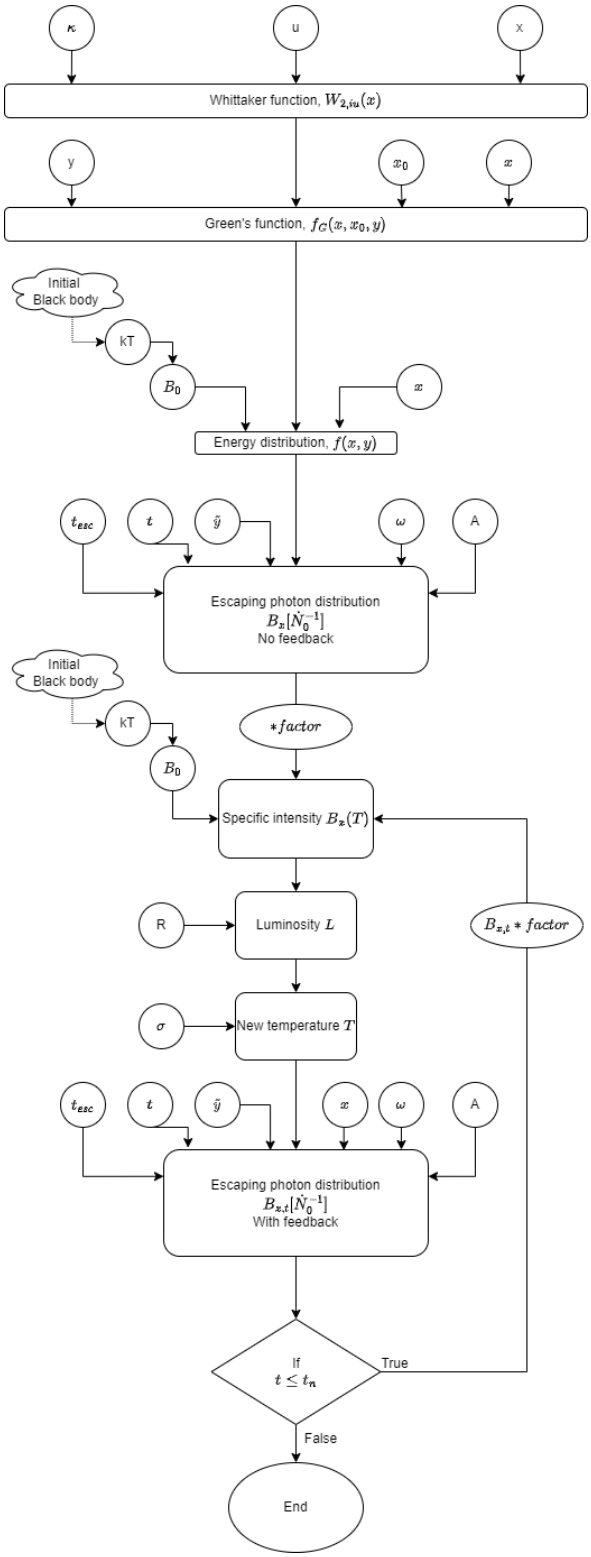

Figure 20: Flowchart of the Python code for the code that creates the time-dependent escaping photon distribution with feedback.